iScience

CellPress
OPEN ACCESS

Article

Dietary caloric restriction protects experimental autoimmune uveitis by regulating Teff/Treg balance

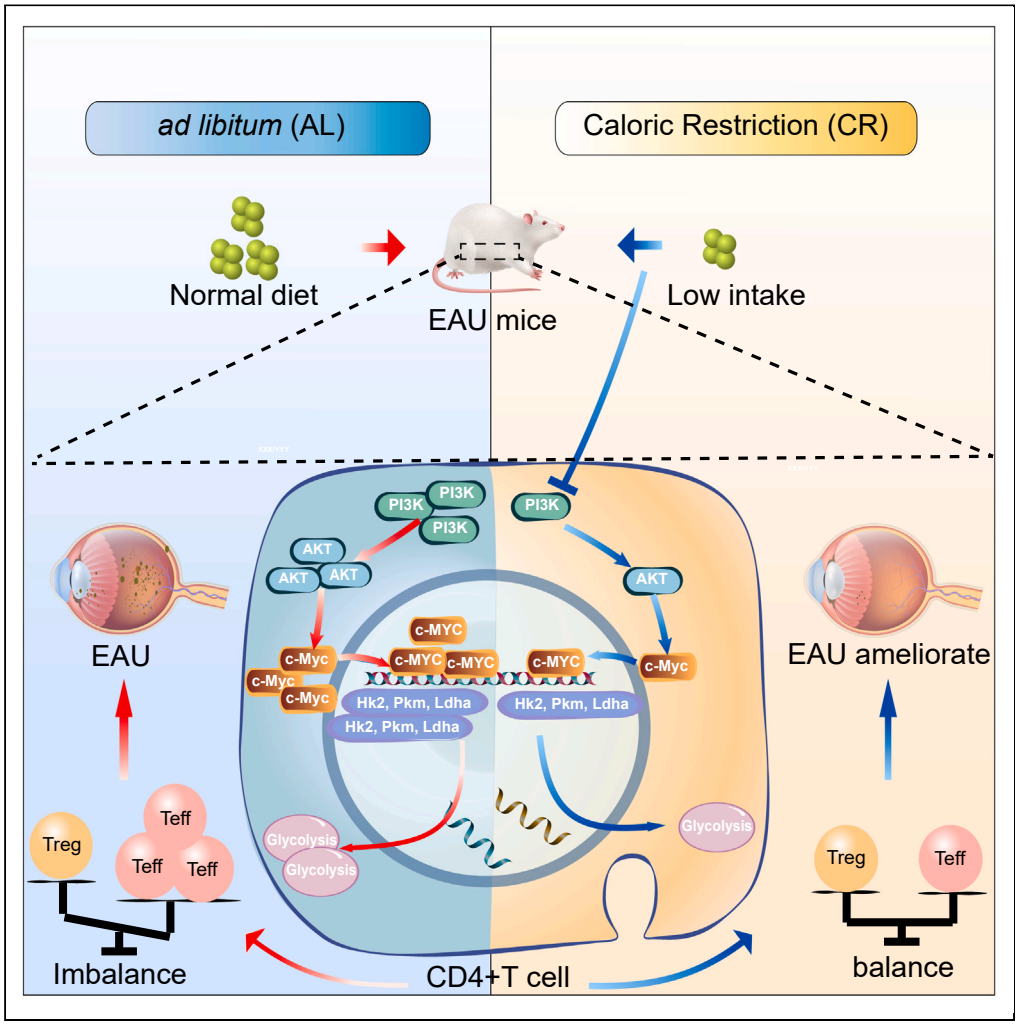

Zhaohuai Li, Runping Duan, Qi Jiang, ..., Wenjun Zou, Ying Lin, Wenru Su

wenjunzou2022@163.com (W.Z.)
linying@gzzoc.com (Y.L.)
suwenru@sjtu.edu.cn (W.S.)

Highlights

A single-cell transcriptomic immune atlas for EAU and CR in lymph nodes

CR alleviated EAU symptoms and regulated Teff/Treg balance

CR influenced the balance of CD4$^+$ T cells by inhibiting the Pi3k/Akt/c-Myc pathway

Li et al., iScience 27, 111279
December 20, 2024
https://doi.org/10.1016/j.isci.2024.111279

iScience

CellPress
OPEN ACCESS

Article

Dietary caloric restriction protects experimental autoimmune uveitis by regulating Teff/Treg balance

Zhaohuai Li,[1,5] Runping Duan,[1,5] Qi Jiang,[2,5] Jiaying Liu,[1,5] Jialing Chen,[3] Loujing Jiang,[1] Tianfu Wang,[1] He Li,[2] Yihan Zhang,[2] Xuening Peng,[1] Zhaohao Huang,[1] Lei Zhu,[1] Wenjun Zou,[4,*] Ying Lin,[1,*] and Wenru Su[2,6,*]

SUMMARY

Uveitis, an autoimmune disease, often leads to blindness. CD4$^+$ T cells, including regulatory T cells (Tregs) and effector T cells (Th1 and Th17), play a critical role in its pathogenesis. Caloric restriction (CR) has been shown to alleviate autoimmune diseases. However, careful characterization of the impact of CR on experimental autoimmune uveitis (EAU) is poorly understood. This study used single-cell RNA sequencing to analyze cervical draining lymph nodes in mice under *ad libitum* (AL) and CR diets, with or without EAU. CR increased Tregs, altered immune cell metabolism, reduced EAU symptoms, and downregulated inflammatory and glycolysis genes. Flow cytometry confirmed CR's inhibitory effect on Th1 and Th17 proliferation and its promotion of Treg proliferation. CR also balanced CD4$^+$ T cells by inhibiting the PI3K/AKT/c-Myc pathway and reducing GM-CSF in Th17 cells. These findings suggest CR as a potential therapeutic strategy for autoimmune diseases.

INTRODUCTION

Uveitis is an autoimmune disease characterized by inflammation within the eye, affecting the central nervous system (CNS).[1–3] It is a significant cause of blindness, accounting for 10–25% of global vision loss, and severe visual impairment or blindness occurs in up to 35% of patients.[4,5] Currently, corticosteroid therapy is the primary treatment approach, which comes with potential long-term side effects. Therefore, gaining a comprehensive understanding of uveitis pathogenesis is essential for the development of effective treatment strategies. Experimental autoimmune uveitis (EAU) serves as an extensively accepted animal model to explore potential pathogenic mechanisms underlying uveitis.[6] T lymphocytes exert a pivotal effect in regulating adaptive immune responses, and their impaired tolerance can lead to the polarization of T cells (TCs) into hyperactive and pathogenic inflammatory phenotypes, contributing to T cell-mediated autoimmune diseases such as uveitis.[1,3] However, the precise mechanisms responsible for T cell polarization into inflammatory phenotypes remain poorly understood. A deeper understanding of intrinsic and extrinsic factors influencing T cell polarization will aid in identifying novel targets for uveitis treatment.

Caloric restriction (CR) is a dietary approach that decreases calorie intake but does not cause malnutrition. It has been demonstrated to modulate nutrient-sensing mechanisms, resulting in improved metabolic profiles, reduced oxidative stress, enhanced stress resistance, suppressed inflammation, and alleviation of metabolic disorders.[7,8] Therefore, it may be a critical strategy for targeting the metabolic system to achieve immune modulation. Nonetheless, the signaling pathways and networks that regulate inflammatory induction across tissues and the impact of CR on EAU are largely unknown and require further investigation.

Lymph nodes play a crucial role in autoimmune processes[9–11] as they serve as sites where distinct immune cells including T cells (TCs), B cells (BCs), as well as dendritic cells (DCs) interact. Lymph nodes facilitate antigen presentation, immune cell activation, and the initiation of autoimmune responses.[12] Among them, cervical-draining lymph nodes (CDLNs) are particularly important for efficient drainage of macromolecules as well as immune cells from the CNS.[13] Consequently, CDLNs may act as production sites for autoreactive TCs as well as BCs targeting CNS autoantigens. In this study, our objective was to employ single-cell RNA sequencing (scRNA-seq) to map the immune cell landscape of CDLNs in mice fed *ad libitum* (AL) or subjected to CR, with or without EAU.

[1]State Key Laboratory of Ophthalmology, Zhongshan Ophthalmic Center, Sun Yat-sen University, Guangdong Provincial Key Laboratory of Ophthalmology and Visual Science, Guangzhou 510060, China
[2]Department of Ophthalmology, Ninth People's Hospital, Shanghai Jiao Tong University School of Medicine, Shanghai 200001, China
[3]Zhongshan School of Medicine, Sun Yat-sen University, Guangzhou 510060, China
[4]Department of Ophthalmology, Wuxi No.2 People's Hospital, Jiangnan University Medical Center, Wuxi, Jiangsu, China
[5]These authors contributed equally
[6]Lead contact
*Correspondence: wenjunzou2022@163.com (W.Z.), linying@gzzoc.com (Y.L.), suwenru@sjtu.edu.cn (W.S.)
https://doi.org/10.1016/j.isci.2024.111279

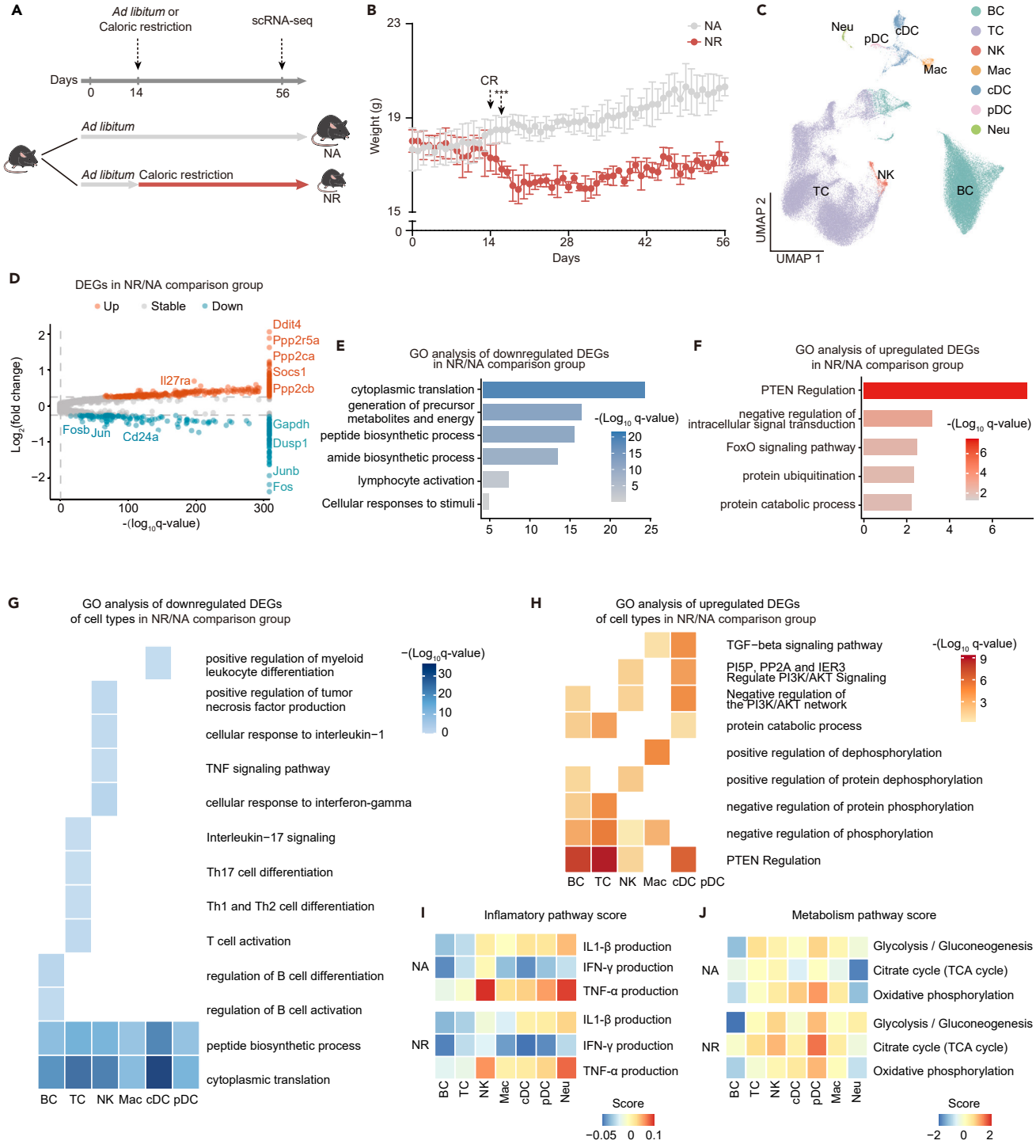

Figure 1. Study design and CR induces complicated and extensive changes in the immune profile of CDLNs

(A) Schematic of the experimental design for single-cell RNA sequencing. CDLNs were harvested from normal (N) mice with *ad libitum* (A) or caloric restriction (R) diet. Samples were processed via scRNA-seq by using the 10x Genomics platform.

(B) Line chart showing weights of NR and NA mice at different time points.

(C) UMAP plot showing clusters of immune cell subsets.

(D) Volcano plot showing upregulated and downregulated DEGs of all immune cell types in the NR/NA comparison group. Red and blue dots indicate upregulated and downregulated DEGs in NR group compared to NA group, respectively.

Figure 1. *Continued*

(E and F) Representative GO terms and KEGG pathways enriched in downregulated (E) or upregulated (F) DEGs of total immune cells in the NR/NA comparison group.

(G and H) Representative GO terms and KEGG pathways enriched in downregulated (G) or upregulated (H) DEGs of immune cell subsets in the NR/NA comparison group.

(I) Heatmap showing average inflammation pathway scores of all immune cell types in NR and NA group.

(J) Heatmap showing average metabolic pathway scores of all immune cell types in NR and NA group.

RESULTS

CR induced complicated and extensive changes within the immune profile of CDLNs

The influence of CR on the immune profile of CDLNs was investigated by generating scRNA-seq data from CDLNs of normal mice with CR (NR) and normal mice with AL (NA) (Figures 1A and S1A). Weight changes in these groups at different time points are shown in Figure 1B. The general effect of CR on the immune profile of CDLNs in normal mice was illustrated. Cell clustering revealed seven immune cell lineages: TCs, BCs, macrophages (Macro), neutrophils (Neu), conventional DC (cDC), plasmacytoid DC (pDC), as well as natural killer cells (NK) based on classical markers (Figures 1C and S1B–S1D). To find out the global gene signatures related to CR in CDLN cells, DEGs were identified for all cell lineages in CDLNs from normal mice. Gene Ontology (GO) analysis of these genes was conducted (Figures 1D–1F). DEG analysis revealed downregulation of Fos, Jun, and Junb in NR mice (Figure 1D). These genes encode components of activator protein 1 (AP-1), which is implicated in various inflammatory pathologies, such as rheumatoid arthritis and psoriasis.[14–16] Gapdh, the main enzyme involved in glycolysis, was also downregulated in NR mice. Conversely, Il27ra, a suppressive regulator of effector Th1 and Th17 cells via its role as the receptor for IL-27, was upregulated in these mice.[17] Ddit4, an mTORC1 inhibitor and a regulator of endoplasmic reticulum stress,[18] was more highly expressed in NR mice than in NA mice (Figure 1D). Ppp2cb, Ppp2ca, and Ppp2r5a were upregulated in NR mice (Figure 1D), encoding protein phosphatase 2A (PP2A) known to inhibit phosphatidylinositol 3-kinase (PI3K)/AKT, dephosphorylate forkhead transcription factor O class 1 (FOXO1), and promote Treg functions.[19] Enrichment analysis revealed that downregulated DEGs among NR mice were related to the biosynthetic processes of the cytoplasm and the activation of the immune system (Figure 1E). Upregulated genes in NR mice were enriched in phosphatase and tensin homolog (Pten) regulation, antigen processing and presentation, and oxidative phosphorylation (Figure 1F). Pten, a tumor suppressor, acts as a negative regulator of PI3K signaling.[20] Collectively, these DEGs and GO analyses indicated a decreased immune effector response, particularly in autoimmunity, and a reduced rate of CDLN glycolysis in NR mice.

Further investigation into cell type-specific transcriptome alterations induced by CR revealed that downregulated DEGs of TCs in NR mice were enriched in the activation as well as the proliferation of TCs, Th17-cell differentiation, and IL-17 signaling pathways (Figure 1G). Meanwhile, negative regulation markers of phosphorylation and PTEN regulation were upregulated (Figure 1H). In BCs, the mitogen-activated protein kinase (MAPK) signaling pathway and the regulation of BC differentiation and activation pathways were downregulated (Figure 1G). Within myeloid cells, cDC as well as pDC from NR mice expressed fewer genes enriched in positive regulation of myeloid leukocyte differentiation and cellular responses to stress (Figure 1G), while these cells highly expressed genes enriched in transforming growth factor (TGF)-beta signaling and negative regulation of PI3K/AKT pathway (Figure 1H). CR-downregulated biological pathways related to the tumor necrosis factor(TNF) signaling pathway, positive regulation of immunity mediated by NK cells, and response to IL-1 were observed in NK cells (Figure 1G), whereas upregulated pathways included PI5P, PP2A, and IER3, which regulate PI3K/AKT signaling and positive regulation of dephosphorylation pathways (Figure 1H). Additionally, proinflammatory cytokine production scores were compared between the two groups. TNF-α, IFN-γ, and IL1-β production scores were significantly decreased in TCs, NK cells, cDC, and macrophages in NR mice compared to NA mice (Figures 1I and S1D–S1F; Table S1). Consistently, the immunoglobulin production score in BCs from NR mice was significantly decreased as well (Figure S1G).

To further investigate the metabolic changes induced by CR, glycolysis or gluconeogenesis, the TCA cycle, and oxidative phosphorylation processes were examined in all cells of the two groups. The results showed that glycolysis or gluconeogenesis was suppressed by CR in all cells, particularly in BCs and TCs (Figures 1J and S1H).

CR induced functional changes of TC and BC compartments in CDLNs

CR induces functional changes in the TC and BC compartments in CDLNs. Lymph nodes primarily consist of T and BCs, which play crucial roles in adaptive immunity. Therefore, our focus was on the alterations induced by CR in both of these cell types.

We categorized eight subtypes of TCs from NR and NA mice based on classical markers, such as naive $CD4^+$ TCs (NCD4), naive $CD8^+$ TCs (NCD8), cytotoxic TCs (CTL), T helper 17 cells (Th17), regulatory TCs (Treg), T follicular helper cells (Tfh), T helper 1 cells (Th1), and proliferative TCs (ProT) (Figures 2A, S2A, and S2B).

The GO analysis demonstrated that downregulated DEGs of Th17 from NR mice were enriched during proinflammatory cytokine production, specifically regulation of TNF production and IFN-γ production, IL-17 signaling pathway, as well as Th17 cell differentiation (Figure 2B). Moreover, the expression of Il17a, Il1r1, and Il23r was decreased in Th17, while TNF-α and IFN-γ production scores were lower in Th1 and Th17 cells from NR mice compared to those from NA mice (Figures 2D, S2C, and 2F), suggesting suppressed function of Th17 cells in NR mice. NCD4 and NCD8 cells exhibited downregulated biological pathways related to MAPK activation, TC activation, and differentiation induced by CR (Figure 2B). Tregs from NR mice highly expressed genes enriched in MAPK activation (Figure 2B), while positive regulation of TC differentiation and activation, TC proliferation, and the T cell receptor (TCR) signaling pathway were upregulated (Figure 2C). Additionally, other

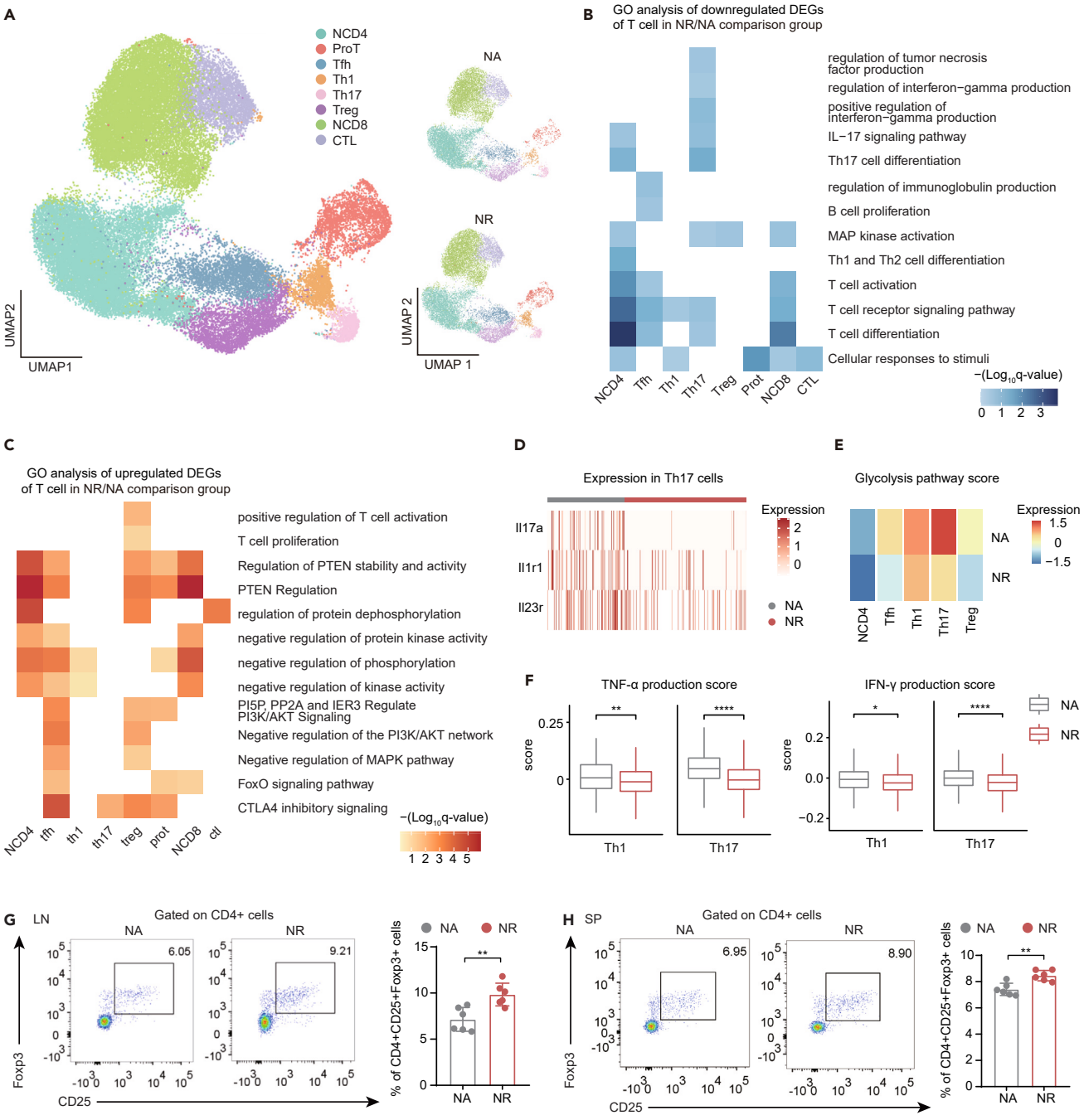

Figure 2. CR induces functional changes of T cell and B cell compartments in CDLNs

(A) UMAP plot showing clusters of T cell subsets from NA and NR mice.

(B and C) Representative GO terms and KEGG pathways enriched in downregulated (B) or upregulated (C) DEGs of T cell subsets in the NR/NA comparison group.

(D) Heatmap showing expression of Il17a, Il1r1, and Il23r in Th 17 cells from NA and NR group.

(E) Heatmap showing average glycolysis pathway scores of T cell subtypes in NR and NA group.

(F) Boxplots showing TNF-α and IFN-γ production score in Th1 and Th17 cells from NA and NR group. Data are represented as mean ± SD. Significance was determined using Wilcoxon rank-sum test. *$p < 0.05$, **$p < 0.01$, ****$p < 0.0001$.

(G and H) Proportions of Treg cells from lymph nodes (LN) (G) or spleen (SP) (H) of NA and NR group were measured by flow cytometry. Each group contains six mice. Data are represented as mean ± SD. Significance was determined using unpaired two-tailed Student's t test. **$p < 0.01$, ***$p < 0.001$, ****$p < 0.0001$.

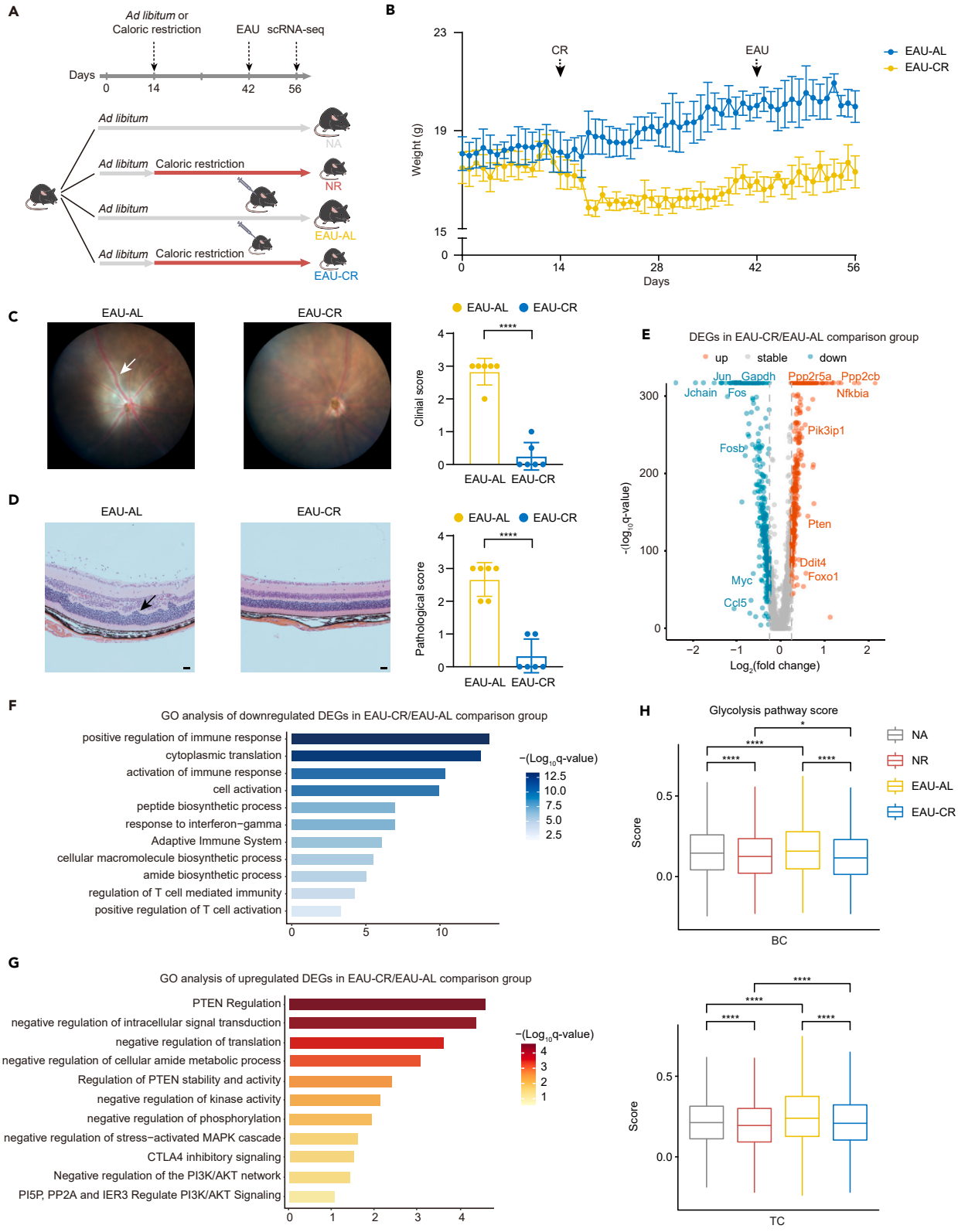
A
Ad libitum or
Caloric restriction
EAU scRNA-seq
Days
0
14
42
56
Ad libitum
NA
Ad libitum Caloric restriction
NR
Ad libitum
EAU-AL
Ad libitum Caloric restriction
EAU-CR
B
CR
EAU
EAU-AL
EAU-CR
Weight (g)
Days
C
EAU-AL
EAU-CR
Clinial score
D
Pathological score
E
DEGs in EAU-CR/EAU-AL comparison group
up
stable
down
Jun
Gapdh
Ppp2r5a
Ppp2cb
Jchain
Fos
Nfkbia
Pik3ip1
Fosb
Pten
Ddit4
Foxo1
Myc
Ccl5
−(log10q-value)
Log2(fold change)
F
GO analysis of downregulated DEGs in EAU-CR/EAU-AL comparison group
positive regulation of immune response
cytoplasmic translation
activation of immune response
cell activation
peptide biosynthetic process
response to interferon−gamma
Adaptive Immune System
cellular macromolecule biosynthetic process
amide biosynthetic process
regulation of T cell mediated immunity
positive regulation of T cell activation
−(Log10q-value)
H
Glycolysis pathway score
NA
NR
EAU-AL
EAU-CR
Score
BC
G
GO analysis of upregulated DEGs in EAU-CR/EAU-AL comparison group
PTEN Regulation
negative regulation of intracellular signal transduction
negative regulation of translation
negative regulation of cellular amide metabolic process
Regulation of PTEN stability and activity
negative regulation of kinase activity
negative regulation of phosphorylation
negative regulation of stress−activated MAPK cascade
CTLA4 inhibitory signaling
Negative regulation of the PI3K/AKT network
PI5P, PP2A and IER3 Regulate PI3K/AKT Signaling
TC

Figure 3. Study design and CR mitigates EAU symptoms and alters immune cell response to EAU challenge

(A) Schematic of the experimental design for single-cell RNA sequencing. CDLNs were harvested from normal (N) mice and EAU.

(E) mice with *ad libitum* (AL) or caloric restriction (CR) diet. Samples were processed via scRNA-seq by using the 10x Genomics platform.

(B) Line chart showing weights of EAU-CR and EAU-AL mice at different time points.

(C) Representative fundus images and clinical scores of eyes from the EAU-AL and EAU-CR group after immunization at day 14. Each group contains six mice. Data are represented as mean ± SD. Significance was determined using unpaired two-tailed Student's t test. ****$p < 0.0001$.

(D) Representative histopathological images (hematoxylin and eosin staining) and pathological scores of eyes from EAU-AL group and EAU-CR group after immunization at day 14. Each group contains six mice. Data are expressed as mean ± SD. Significance was determined using unpaired two-tailed Student's t test. ****$p < 0.0001$. Scale bars, 20 μm.

(E) Volcano plot showing upregulated and downregulated DEGs of all immune cell types in the EAU-CR/EAU-AL comparison group. Red and blue dots indicate upregulated and downregulated DEGs in NR group compared to NA group, respectively.

(F and G) Representative GO terms and KEGG pathways enriched in downregulated (F) or upregulated (G) DEGs of total immune cells in the EAU-CR/EAU-AL comparison group.

(H) Boxplots showing average glycolysis pathway scores of BC and TC in NR, NA, EAU-CR, and EAU-AL group. Data are represented as mean ± SD. Significance was determined using Wilcoxon rank-sum test. *$p < 0.05$, ****$p < 0.0001$.

TC subtypes in NR mice showed upregulated genes related to pathways such as PTEN regulation, regulation of dephosphorylation and phosphorylation, negative regulation of the PI3K/AKT network, and FOXO signaling pathway (Figure 2C).

Flow cytometry confirmed that CR treatment increased $CD4^+$ Foxp3+ TCs in NR mice (Figures 2G and 2H), but led to no change in the proportion of $CD4^+$ IL17A + T as well as $CD4^+$ IFN-γ+ TCs (Figures S2F–S2I), which was observed in both lymph nodes and spleens. Furthermore, we investigated metabolic alterations in CR-induced TCs. The glycolysis pathway score in NCD4, Tfh, Th17, and Treg cells from NR mice was significantly lower compared to that in NA mice (Figures 2E and S2D). Moreover, inflammatory genes such as Fos, Junb, and Pim1, as well as glycolysis-related genes like Gapdh, were expressed less in NR mice. Conversely, Ppp2ca, Ppp2cb, Ppp2r5a, and Pik3ip1 were more expressed in these mice relative to their counterparts (Figure S2E). To further elucidate the role of glycolysis in the anti-inflammatory effects of CR, we assessed the expression levels of key glycolytic molecules and enzymes. Our findings indicated that CR reduced the expression levels of HK2, PKM2, and LDHA in Th17 cells (Figures S2K–S2M), but led to no change in the expression levels of c-Myc in Th17 cells (Figure S2J).

These findings indicate that TCs in CR-induced CDLNs exhibited anti-inflammatory and regulatory phenotypes while displaying decreased autoimmune ability. Thus, CR may induce various immune alterations in different TC subsets and suppress glycolysis in these cells. We also observed impaired Th17 cell function in CR-induced CDLNs.

Regarding BC compartments, we identified three subtypes of BCs from NR and NA mice based on classical markers: naive BCs (NBC), germinal center BCs (GC), and plasma cells (PC) (Figures S3A–S3D). The GO analysis of BCs demonstrated that the upregulated DEGs were enriched in PTEN pathways and regulation of dephosphorylation in NBC, as well as PI3K/AKT signaling in GBC (Figure S3E). CR downregulated regulation of BC proliferation and activation, MAPK signaling pathway, regulation of BC receptor signaling pathway, and regulation of translation in BCs, particularly in NBC (Figure S3F). We then examined the metabolic changes among BCs and found that the glycolysis pathway score induced by CR was significantly lower in GC and NBC compared to AL (Figure S3G). Similarly to TCs, the changes in gene expression in BCs from NR mice showed similar tendencies, including Ppp2r5a, Ppp2ca, and Gapdh (Figures S3H and S3I). Thus, CR may suppress the primary functions of BCs.

CR mitigated EAU symptoms and altered immune cell response to the challenge of EAU

To understand this phenomenon and further investigate the relationship between CR and EAU, we conducted an analysis of changes in autoimmune responses during EAU in mice subjected to CR (Figure 3A). We assessed the weights of EAU mice with CR (EAU-CR) and with AL (EAU-AL) at different time points and documented the severity of EAU symptoms using a published clinical grading scale.[21] Evaluation of the eyes using a fundus camera revealed multiple chorioretinal lesions and/or infiltration as manifestations of EAU (Figure 3C). Upon histological examination of sectioned eyeballs stained with H&E, we observed inflammatory infiltration together with retinal folding within the EAU lesions (Figure 3D). EAU-CR mice showed milder symptoms of EAU, characterized by lower clinical and pathological scores, in contrast with EAU-AL mice (Figures 3C and 3D).

We performed single-cell analysis on the CDLNs of EAU-CR and EAU-AL mice, as depicted in Figure 3A. Using classical markers, we identified the major immune cell clusters, as shown in and Figures S4A, S1A and S1B. Our initial analysis focused on identifying DEGs between EAU-CR and EAU-AL mice. We observed similar changes in DEGs as those observed in NR mice compared to NA mice, such as Gapdh, Ppp2ca, Pim1, and Pik3ip1 (Figures 3E and S4B). GO analysis revealed downregulation of positive regulation of immune response, cell activation, and translation pathways (Figure 3F), while upregulated pathways included PTEN regulation, negative regulation of the PI3K/AKT network, and negative regulation of phosphorylation (Figure 3G). Additionally, CR attenuated the EAU-induced increase in glycolysis pathway scores in both T and BCs (Figure 3H).

We proceeded to investigate the influence of CR on the response of TC subsets to the EAU challenge. We identified eight TC subsets in EAU-CR and EAU-AL mice, similar to those found in normal mice (Figure S4C). To gain insights into the functional alterations induced by CR in response to EAU, we conducted GO analysis on these TC subsets (Figures S4D and S4E). Our findings revealed downregulation of MAPK signaling, NF-κB signaling, as well as PI3K/AKT signaling pathways, while the PTEN regulation pathway was upregulated in the T cell subsets of EAU-CR mice (Figures S4D and S4E). Additionally, we observed downregulated pathways associated with inflammation (annotated as

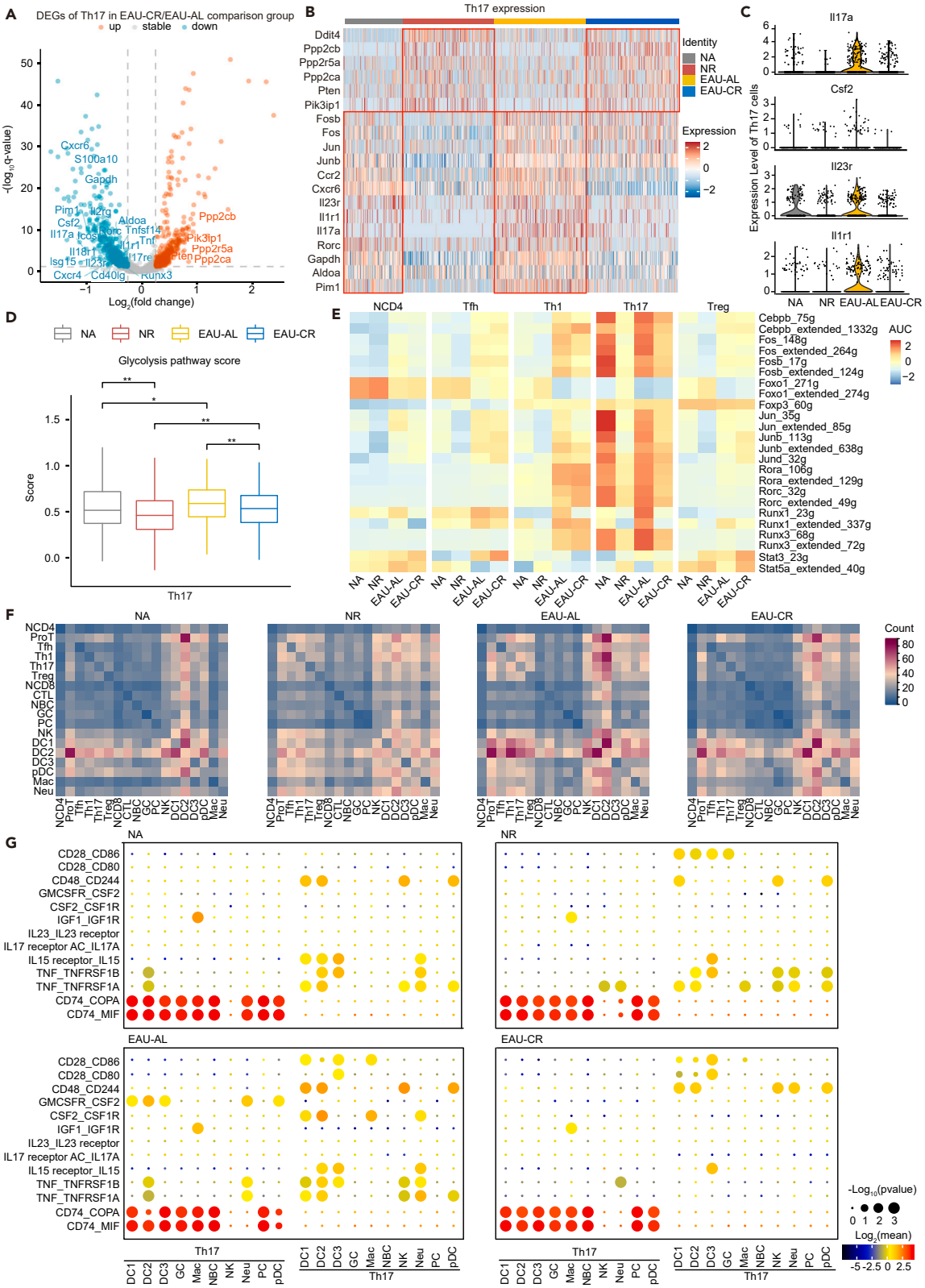
A
DEGs of Th17 in EAU-CR/EAU-AL comparison group
up
stable
down
-(log10 q-value)
Log2(fold change)
Cxcr6
S100a10
Gapdh
Pim1
Il2rg
Csf2
Aldoa
Il17a
Icos
Tnfsf14
Il1r1
Tnf
Il18r1
Il17re
Isg15
Il23a
Cxcr4
Cd40lg
Runx3
Ppp2cb
Pik3ip1
Ppp2r5a
Pten
Ppp2ca
B
Th17 expression
Ddit4
Ppp2cb
Ppp2r5a
Ppp2ca
Pten
Pik3ip1
Fosb
Fos
Jun
Junb
Ccr2
Cxcr6
Il23r
Il1r1
Il17a
Rorc
Gapdh
Aldoa
Pim1
Identity
NA
NR
EAU-AL
EAU-CR
Expression
C
Il17a
Csf2
Il23r
Il1r1
Expression Level of Th17 cells
NA
NR
EAU-AL
EAU-CR
D
NA
NR
EAU-AL
EAU-CR
Glycolysis pathway score
Score
Th17
E
NCD4
Tfh
Th1
Th17
Treg
Cebpb_75g
Cebpb_extended_1332g
Fos_148g
Fos_extended_264g
Fosb_17g
Fosb_extended_124g
Foxo1_271g
Foxo1_extended_274g
Foxp3_60g
Jun_35g
Jun_extended_85g
Junb_113g
Junb_extended_638g
Jund_32g
Rora_106g
Rora_extended_129g
Rorc_32g
Rorc_extended_49g
Runx1_23g
Runx1_extended_337g
Runx3_68g
Runx3_extended_72g
Stat3_23g
Stat5a_extended_40g
AUC
F
NA
NR
EAU-AL
EAU-CR
Count
NCD4
ProT
Tfh
Th1
Th17
Treg
NCD8
CTL
NBC
GC
PC
NK
DC1
DC2
DC3
pDC
Mac
Neu
G
NA
NR
EAU-AL
EAU-CR
CD28_CD86
CD28_CD80
CD48_CD244
GMCSFR_CSF2
CSF2_CSF1R
IGF1_IGF1R
IL23_IL23 receptor
IL17 receptor AC_IL17A
IL15 receptor_IL15
TNF_TNFRSF1B
TNF_TNFRSF1A
CD74_COPA
CD74_MIF
Th17
-Log10(pvalue)
Log2(mean)

Figure 4. CR-induced alterations in T cell subsets and cell-cell communication

(A) Volcano plot showing upregulated and downregulated DEGs of Th17 cells in the EAU-CR/EAU-AL comparison group. Red and blue dots indicate upregulated and downregulated DEGs in NR group compared to NA group, respectively.

(B) Heatmap showing gene expression in Th17 cells of NA, NR, EAU-AL, and EAU-CR group.

(C) Violin plots showing the expression of Il17a, Csf2, Il23r, and Il1r1 in Th17 cells of NA, NR, EAU-AL, and EAU-CR group.

(D) Boxplot showing average glycolysis pathway scores of Th17 cells in NR, NA, EAU-CR, and EAU-AL group. Data are represented as mean ± SD. Significance was determined using Wilcoxon rank-sum test. *$p < 0.05$, **$p < 0.01$.

(E) Heatmap showing single-cell regulon scores inferred by SCENIC in T cell subtypes of NA, NR, EAU-AL, and EAU-CR group (g, genes; extended, SCENIC-annotated additional genes).

(F) Heatmap showing the number of possible interactions between immune cells analyzed in NA, NR, EAU-AL and EAU-CR groups.

(G) The interaction of Th17 cells with myeloid cells and B cells in NA, NR, EAU-AL and EAU-CR mice.

positive regulation of IFN-γ production, positive regulation of cytokine production, along with IL-17 signaling pathway) and immune responses (annotated as TC differentiation and activation, and positive regulation of the immune response) in EAU-CR mice (Figure S4E). These results suggest that CR induces a suppressive immune process and mitigates the severity of inflammation in response to the challenge of EAU. Changes in gene expression were further explored, specifically in Th17 cells among the four groups. Differential expression analysis of Th17 cells between EAU-CR and EAU-AL mice revealed genes affected by CR, including Ppp2cb, Pik3ip1, Pim1, and Gapdh (Figures 4A and 4B). Moreover, the expression of Il17a, Il23r, and Il1r1, which were increased during the EAU challenge, was reduced in Th17 cells by CR (Figures 4A and 4B, and 4C), indicating a restrained function of Th17 cells induced by CR. Notably, CR also decreased the glycolysis pathway score in Th17 cells, both in normal and EAU mice, which exhibited enhancement during the EAU response (Figure 4D). Furthermore, we assessed the expression levels of transcription factors in the four groups. Transcription factors associated with Th17 differentiation and function showed reduced expression in Th17 cells induced by CR, such as Jun, Runx1, Rora, and Rorc (Figures 4E and S4F). Conversely, Treg cells exhibited enhanced expression of Foxo1 and Stat3 under CR conditions (Figure 4E). Therefore, it appears that CR weakens the role of Th17 cells and promotes immunosuppression during EAU development.

We also classified three subtypes of BCs in EAU-CR and EAU-AL mice based on classical markers: NBC, GC, and PC (Figure S5A). GO analysis conducted on BCs revealed upregulated pathways enriched in PTEN pathways, negative regulation of dephosphorylation, and negative regulation of immune system processes, particularly in GBCs (Figure S5B). Downregulated pathways included BC proliferation, differentiation, activation, and immune effector processes (Figure S5C). Furthermore, the glycolysis pathway score, which may be enhanced in EAU mice, was reduced in these BC subtypes under CR conditions, especially in NBCs (Figure S5D).

In summary, our findings elucidated the alterations in TC and BC subsets in the CDLNs in response to the challenge of EAU, in normal mice as well as EAU mice. CR resulted in a mitigated inflammatory status, a suppressive immune response process, and a restrained role of Th17 cells during the EAU challenge. Moreover, the reduction in the glycolysis process induced by CR suggested decreased activation of immune cells, potentially contributing to the amelioration of EAU symptoms.

CR alleviated aberrant intercellular communication in EAU

To understand the intercellular communication among immune cells in the four groups, the cell-cell communication network was explored utilizing CellphoneDB2 analysis (Figures 4F, 4G and S6A). We found that the enhanced interactions observed in response to EAU were rescued by CR, specifically the interactions involving Th17 cells and other immune cells (Figures 4F and 4G). Notably, the interaction between CSF2 and its receptors, which is known to be associated with CNS autoimmunity, occurred between Th17 cells and myeloid cells after EAU development and was suppressed by CR (Figure 4G). Additionally, the interactions involving CD244 and CD48, IL-15R and IL-15, as well as IGF1 and IGF1R between Th17 cells and myeloid cells or macrophages were reduced under CR conditions (Figure 4G). These findings suggest that the activation and function of Th17 cells were suppressed by CR.

Further analysis revealed that the reduction in interaction pairs observed during EAU development, such as the interaction between TGFB1 and its receptors, was enhanced by CR (Figure S6A), indicating a higher immunosuppressive status induced by CR in EAU mice. Interactions associated with proinflammatory cytokines, such as IL1R2, CCL8, and CCR5, were enhanced after EAU development (Figure S6A). Interestingly, the interaction involving CCL7 and its receptors between macrophages and other cells, which can amplify the inflammatory process, was decreased in EAU-CR mice compared to EAU-AL mice (Figure S6A). These results further demonstrate that CR attenuates the inflammatory process.

CR suppressed inflammatory status and reduces Th17 pathogenicity via PI3K/AKT/c-Myc axis

The analysis of DEGs and GO revealed that CR induces the attenuation of inflammation and immune processes. We utilized flow cytometry to validate these responses and changes. Our findings demonstrated that CR decreased the population of Th1 (IFN-γ+) cells as well as Th17 (IL-17A+) cells, while increasing the number of Treg (Foxp3+) cells during the development of EAU. Moreover, CR resulted in decreased expression of inflammatory and pathogenic factors. These observations confirmed the suppressive inflammatory status and immune process induced by CR (Figures 5A–5J).

To identify the impact of CR on Th17 cell's function, which was essential for the pathogenicity of AU,[22] we analyzed the DEGs specifically in Th17 cells among the four groups. The expression levels of Il17a, Csf2, as well as Il23r were lower among Th17 cells from CR mice compared to those from AL mice following EAU development (Figures 4A–4C). Additionally, flow cytometry analysis showed reduced production of

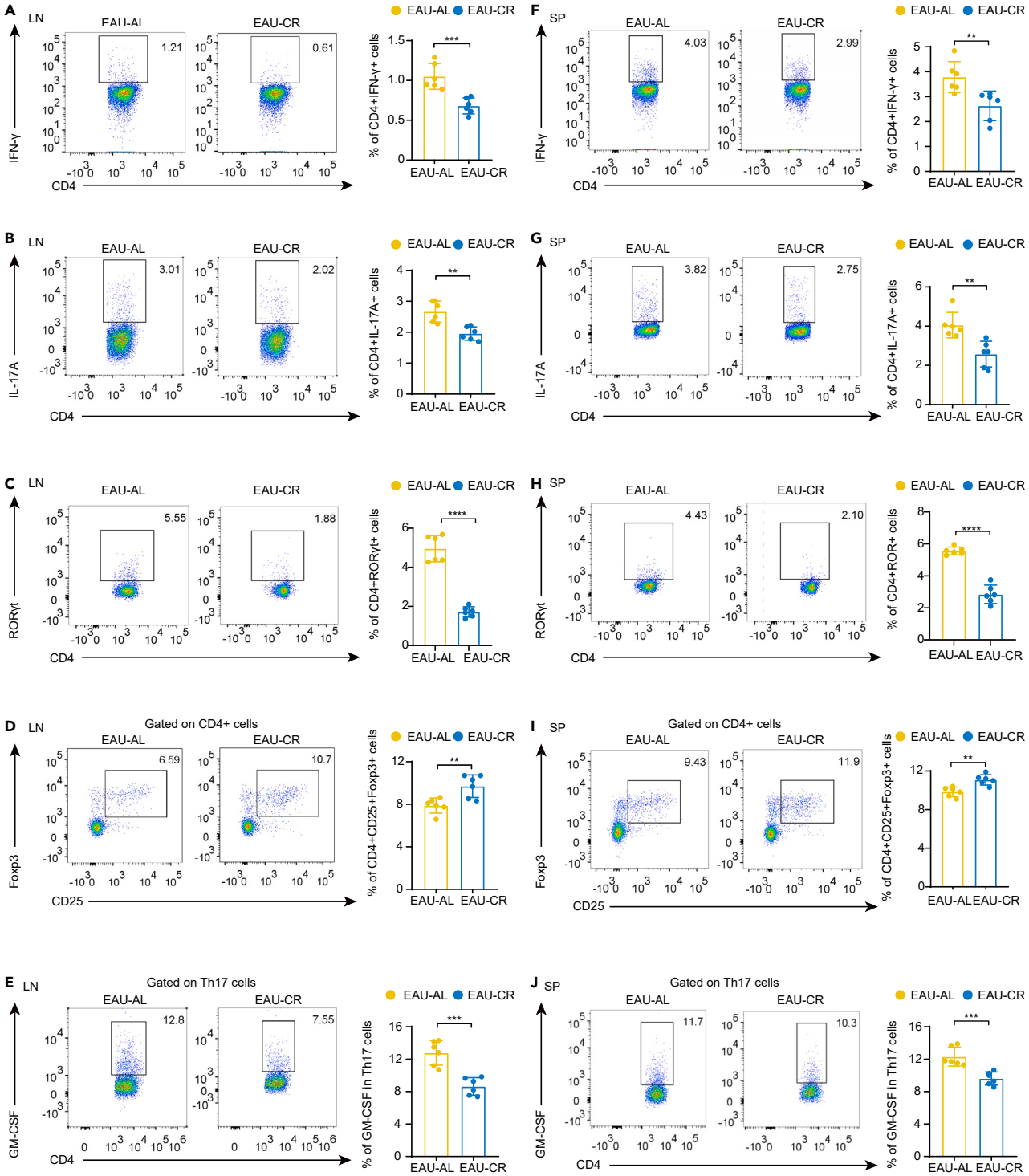

Figure 5. CR weakened Th17 pathogenicity

(A–E) Proportions of Th1 cells (A), Th17 cells (B and C), regulatory T cells (Treg) (D) and GM-CSF+ Th17 cells (E) from LN of EAU-AL and EAU-CR group were measured by flow cytometry. Each group contains six mice. Data are represented as mean ± SD. Significance was determined using unpaired two-tailed Student's t test. $^{**}p < 0.01$, $^{***}p < 0.001$.

(F–J) Proportions of Th1 cells (F), Th17 cells (G and H), regulatory T cells (Treg) (I) and GM-CSF+ Th17 cells (J) from spleen (SP) of EAU-AL and EAU-CR group were measured by flow cytometry. Each group contains six mice. Data are represented as mean ± SD. Significance was determined using unpaired two-tailed Student's t test. $^{**}p < 0.01$, $^{***}p < 0.001$.

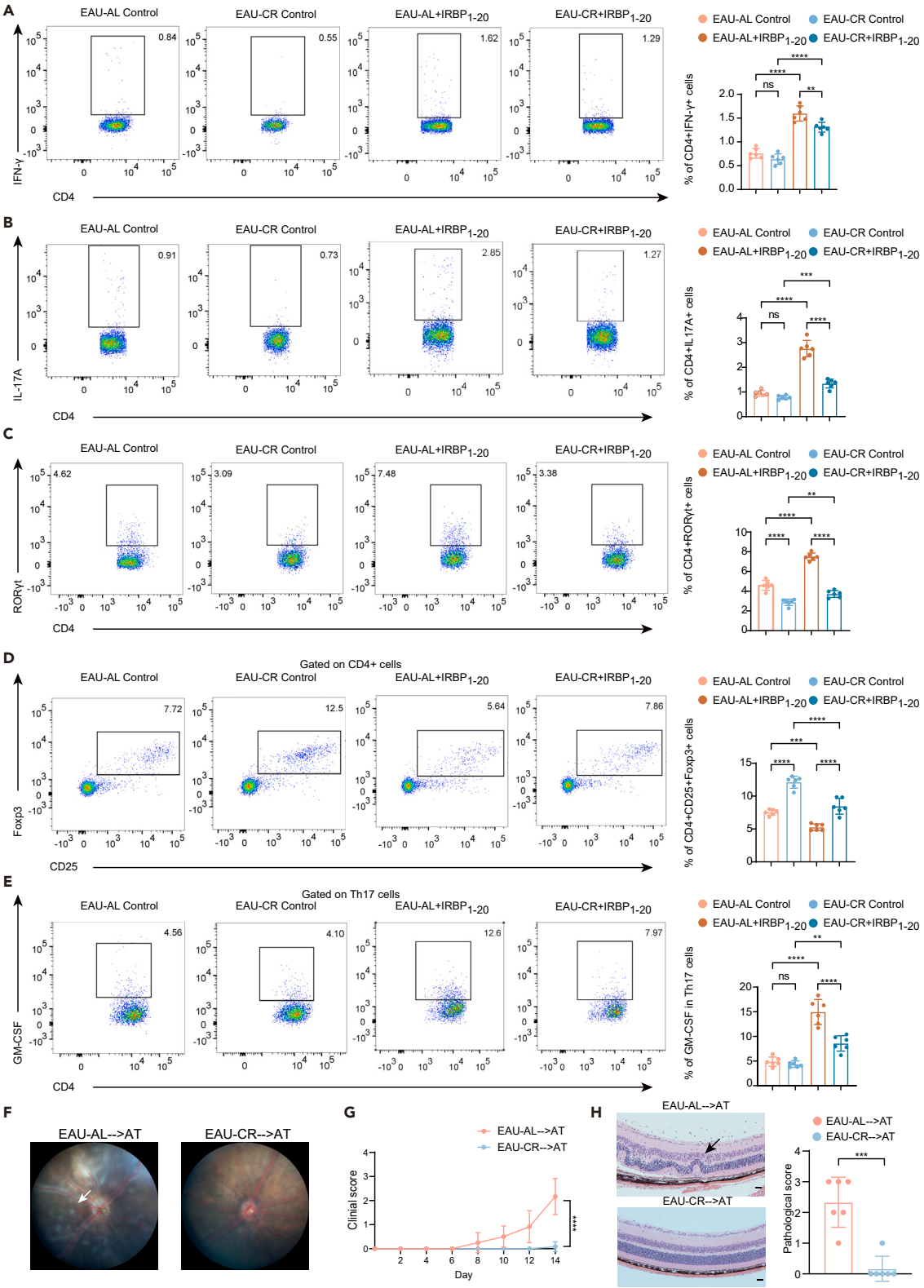
A
EAU-AL Control
EAU-CR Control
EAU-AL+IRBP1-20
EAU-CR+IRBP1-20
0.84
0.55
1.62
1.29
IFN-γ
CD4
% of CD4+IFN-γ+ cells
B
0.91
0.73
2.85
1.27
IL-17A
CD4
% of CD4+IL17A+ cells
C
4.62
3.09
7.48
3.38
RORγt
CD4
% of CD4+RORγt+ cells
D
Gated on CD4+ cells
7.72
12.5
5.64
7.86
Foxp3
CD25
% of CD4+CD25+Foxp3+ cells
E
Gated on Th17 cells
4.56
4.10
12.6
7.97
GM-CSF
CD4
% of GM-CSF in Th17 cells
F
EAU-AL-->AT
EAU-CR-->AT
G
Clinial score
Day
H
Pathological score

Figure 6. CR weakened IRBP-specific Teff differentiation

(A–E) CDLNs cells from EAU-AL and EAU-CR group cultured with or without $IRBP_{1-20}$ for 72 h. Proportions of Th1 cells (A), Th17 cells (B and C), regulatory T cells (Treg) (D) and GM-CSF+ Th17 cells (E) of EAU-AL and EAU-CR group were measured by flow cytometry. Data are represented as mean ± SD from six independent experiments. Significance was determined using unpaired two-tailed Student's t test. $^{**}p < 0.01$, $^{***}p < 0.001$, $^{****}p < 0.0001$.

(F) The representative fundus images after induction by $CD4^+$ T cells from EAU-AL (EAU-AL– > AT) or EAU-CR (EAU-CR– > AT) groups after immunization at day 14.

(G) Clinical scores of EAU-AL– > AT and EAU-CR– > AT groups ($n = 6$). Clinical scores significantly decreased ($^{****}p < 0.0001$) in EAU-CR– > AT group compared to EAU-AL– > AT group at day 14. Data are shown as mean ± SD from three independent experiments. Data were analyzed using unpaired student t tests.

(H) The representative HE staining images and pathological scores after induction by $CD4^+$ T cells from EAU-AL (EAU-AL– > AT) or EAU-CR (EAU–>CR-AT) groups after immunization at day 14. Scale bars, 20 μm. Each group contains six mice. Significance was determined using unpaired Student's t test. $^{***}p < 0.001$.

granulocyte-macrophage colony stimulating factor (GM-CSF), predominantly secreted by Th17 cells along with a characteristic feature distinguishing pathogenic Th17 cells from non-pathogenic ones,[23] in the lymph nodes and spleens of EAU mice subjected to CR (Figures 5E and 5J). Collectively, these results indicate impaired Th17 pathogenicity resulting from CR during EAU.

To further confirm these findings within the $IRBP_{1-20}$-specific response, CDLN cells were collected from EAU-CR and EAU-AL mice, cultured with $IRBP_{1-20}$ as a stimulator, and we observed a decrease in the number of Th1, Th17, and in the expression of GM-CSF, due to CR (Figures 6A–6C, and 6E). Additionally, the proportion of Tregs was elevated among EAU-CR mice (Figure 6D). Furthermore, through adoptive transfer experiments, we found that $CD4^+$ TCs obtained from CDLNs of EAU-AL mice successfully induced EAU, while those from EAU-CR mice failed among normal mice (Figures 6F and 6G). We obtained similar results using an alternative method to induce $IRBP_{1-20}$-specific T cells[24] (Figures S7B–S7G).

To investigate whether the specific mechanism by which CR effectively inhibits EAU-related inflammation is related to glycolysis, we further conducted an analysis of single-cell data. Our findings revealed that the expression levels of glycolysis-related genes, such as Pik3r1, Akt1, Myc, and Hif1α, as well as key glycolytic enzymes, were significantly elevated in the presence of EAU and were notably reduced following CR treatment (Figure S6B). This trend was confirmed through flow cytometry analysis (Figures 7A–7D). In summary, these results collectively indicate that CR effectively restrains inflammatory and immune processes, as well as weakens the pathogenicity of Th17 cells, via PI3K/AKT/c-Myc/glycolysis axis.

DISCUSSION

In our study, we have elucidated the transcriptomic shifts within CDLNs of mice subjected to CR and their subsequent response to EAU. Our findings underscore the modulatory role of CR in immune cell dynamics, particularly in dampening the pathogenicity of Th17 cells, which is pivotal in mitigating EAU symptoms. CR was found to influence the PI3K/AKT/c-Myc signaling axis and the glycolytic pathway, thereby altering Th17/Treg cell differentiation and restoring T cell homeostasis.

Cellular metabolism, including aerobic glycolysis, fatty acid oxidation, and oxidative phosphorylation, is crucial for T cell fate determination.[25] Recent studies indicate that enhanced glycolysis in immune cells is essential for effective processes, such as cell activation, proliferation, and effector responses.[26] Nutrient metabolism significantly influences the differentiation and function of various immune cells. Dietary interventions like calorie restriction, time-restricted eating, and fasting can modulate immune cell function.[8] Previous research has shown that CR can reduce the expression of inflammatory cytokines associated with EAU.[27] Our study offers a detailed analysis of the mechanisms by which CR alleviates EAU through a comprehensive immune cell map. We found that CR regulates Th17 and Treg cell differentiation by affecting the glycolytic pathway via the PI3K/AKT/c-Myc/glycolysis axis and restores T cell homeostasis by reshaping the immune microenvironment.

The activation of effector TCs (Teff cells) heavily relies on the PI3K/AKT/mTOR signaling pathway. Conversely, the low-energy state induced by CR suppresses the PI3K/AKT/mTOR axis while reciprocally activating adenosine monophosphate-activated protein kinase (AMPK).[28–30] The hypoglycemia induced by CR reduces anabolic hormones and inhibits insulin-dependent anabolic metabolism by impeding the PI3K and MAPK signaling pathways, thereby preventing mTOR activation. Inactivated mTOR triggers autophagy, contributing to the suppression of inflammation by downregulating IFN/proinflammatory cytokine secretion, as well as inhibiting inflammasome activity.[31] Besides, inactivation of mTOR hampers hypoxia-inducible factor 1 (HIF-1)-dependent activation of genes in relation with inflammation, the proinflammatory effects of reactive oxygen species (ROS), as well as NF-κB activation.[32,33] The inhibition of the PI3K signaling pathway entails critical metabolic consequences, including increased lipolysis and ketogenesis, together with a shift in substrate utilization for energy production from glucose to fatty acids and ketone bodies.[34] Our study employed single-cell metabolic analysis, which revealed reduced glycolytic metabolic pathway activity during CR. We observed downregulation in the expression of glycolysis-related genes such as Gapdh and Pim1, along with increased expression of inhibitors of the PI3K/AKT/mTOR/glycolysis pathway, including Pten, Pik3ip1, and PP2A-related genes, in TCs and BCs.

Although previous studies have extensively investigated alterations in the immune system during CR using scRNA sequencing in various rat organs,[35] a comprehensive immune cell atlas of CR lymph nodes, which play a crucial role in immune responses, was lacking prior to our study. Furthermore, detailed investigations of cellular changes in CR CDLNs and their association with autoimmune diseases were also lacking. Therefore, our study fills these knowledge gaps and provides valuable insights into the single-cell expression landscape of EAU and CR.

Consistent with previous research highlighting the anti-inflammatory effects of CR in age-related inflammation and other eye diseases,[36–39] our study demonstrated that CR can attenuate the inflammatory response of immune cells within CDLNs, particularly during

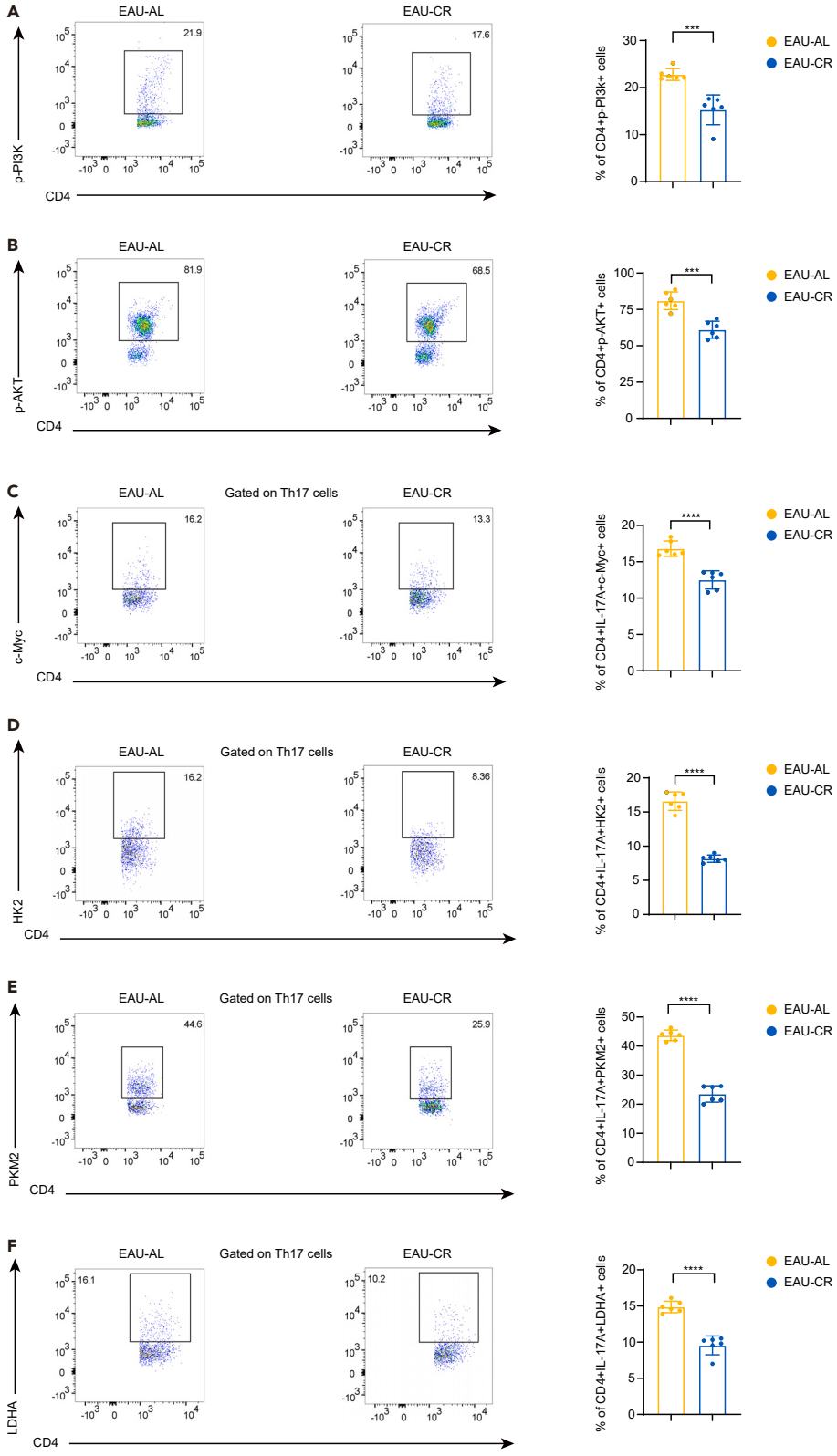
A
EAU-AL
EAU-CR
21.9
17.6
p-PI3K
CD4
% of CD4+p-PI3k+ cells
***
EAU-AL
EAU-CR
B
EAU-AL
EAU-CR
81.9
68.5
p-AKT
CD4
% of CD4+p-AKT+ cells
***
EAU-AL
EAU-CR
C
EAU-AL
Gated on Th17 cells
EAU-CR
16.2
13.3
c-Myc
CD4
% of CD4+IL-17A+c-Myc+ cells
****
EAU-AL
EAU-CR
D
EAU-AL
Gated on Th17 cells
EAU-CR
16.2
8.36
HK2
CD4
% of CD4+IL-17A+HK2+ cells
****
EAU-AL
EAU-CR
E
EAU-AL
Gated on Th17 cells
EAU-CR
44.6
25.9
PKM2
CD4
% of CD4+IL-17A+PKM2+ cells
****
EAU-AL
EAU-CR
F
EAU-AL
Gated on Th17 cells
EAU-CR
16.1
10.2
LDHA
CD4
% of CD4+IL-17A+LDHA+ cells
****
EAU-AL
EAU-CR

Figure 7. CR repressed PI3K/AKT/c-Myc/glycolysis pathway

(A–F) The proportions of $CD4^+$ p-PI3K+ cells (A), $CD4^+$ *p*-AKT+ cells (B), CD4+IL-17A+c-Myc+ T cells (C), CD4+IL-17A + HK2+ T cells (D), CD4+IL-17A + PKM2+ T cells (E), and CD4+IL-17A+LDHA+ T cells (F) were measured by flow cytometry. Each group contains six mice. Data are represented as mean ± SD. Significance was determined using unpaired two-tailed Student's t test. ***$p < 0.001$, ****$p < 0.0001$.

autoimmune challenges. Specifically, TCs exhibited reduced proliferation, activation, IL-17 signaling, along with differentiation toward Th17 cells. BCs showed decreased production of immunoglobulins, and other innate immune cells displayed lower levels of inflammation-associated pathways. GO analysis revealed impaired cell activation among T cell subsets as well as compromised antigen presentation and cell division among BC subsets. Within the various immune cell types, Th1, Th17, and Treg cells are recognized as key contributors to either uveitis or other autoimmune diseases.[22,40,41] In the present study, CR suppressed the proliferation of Th1/Th17 cells while promoting the expansion of Treg cells. Notably, the pathogenicity of Th17 cells was diminished, as evidenced by reduced secretion of GM-CSF in CR mice.

Limitations of the study

Our findings offered novel ideas into the intricate interaction of CR and autoimmunity, serving as valuable knowledge for researchers interested in this field of study. However, there are some limitations in this study. Firstly, the absence of human AU samples, such as the correlation between body mass index (BMI) and AU scores or other disease activity indicators, limits the direct clinical applicability and transformative potential of our findings. Secondly, while a decrease in glucose metabolism was noted, the study did not delve into other metabolic profiles, including amino acids and lipids, in serum or cell lysates for both human and murine samples. Additionally, the translation of these findings into potential treatments for human patients with AU, such as clinical trials for CR treatment, remains to be explored.

RESOURCE AVAILABILITY

Lead contact

Further information and requests for resources and reagents should be directed to and will be fulfilled by the lead contact, Wenru Su (suwr3@mail.sysu.edu.cn).

Materials availability

This study did not generate new unique reagents.

Data and code availability

- Single-cell RNA-seq data have been deposited at Genome Sequence Archive (GSA) and are publicly available as of the date of publication. Accession numbers: CRA016398.
- This paper does not report original code.
- Any additional information required to reanalyze the data reported in this paper is available from the lead contact upon request.

ACKNOWLEDGMENTS

This work was supported by grants from the National Science Fund for Outstanding Young Scholars (82122016), National Natural Science Foundation of China (823B2019), the China Postdoctoral Science Foundation (2023TQ0393), Postdoctoral Fellowship Program of CPSF (GZB20230883), Science and Technology Program of Guangzhou, China (SL2022A03J00452), Top Talent Support Program for young and middle-aged people of Wuxi Health Committee (BJ2023036).

AUTHOR CONTRIBUTIONS

W.S., Y.L., and W.Z designed the study. Z.L., R.D., and Q.J. conducted the experiment and acquired the data. J.L., J.C., and Y.Z. analyzed the data and prepared the figures. Z.L., L.J., T.W., and H.L. wrote the manuscript. X.P., Z.H., and L.Z. assisted the experiments and performed the statistical analyses. The manuscript was reviewed by all authors. Order of co-first author is based on the length of time spent on the project.

DECLARATION OF INTERESTS

The authors declare no competing interests.

STAR★METHODS

Detailed methods are provided in the online version of this paper and include the following:

- KEY RESOURCES TABLE
- EXPERIMENTAL MODEL AND STUDY PARTICIPANT DETAILS
  - Mice
- METHOD DETAILS
  - Caloric restriction
  - EAU model induction and clinical score
  - Histopathologic assessment
  - Treatment of CDLNs
  - Flow cytometry analysis
  - Adoptive transfer of $CD4^+$ TCs
  - scRNA sequencing and analysis
  - DEG analysis

SUPPLEMENTAL INFORMATION

Supplemental information can be found online at https://doi.org/10.1016/j.isci.2024.111279.

Received: May 2, 2024
Revised: July 29, 2024
Accepted: October 25, 2024
Published: October 28, 2024

REFERENCES

1. Wildner, G., and Diedrichs-Möhring, M. (2019). Resolution of uveitis. Semin. Immunopathol. *41*, 727–736. https://doi.org/10.1007/s00281-019-00758-z.
2. Iwase, A., Araie, M., Tomidokoro, A., Yamamoto, T., Shimizu, H., and Kitazawa, Y.; Tajimi Study Group (2006). Prevalence and causes of low vision and blindness in a Japanese adult population: the Tajimi Study. Ophthalmology *113*, 1354–1362. https://doi.org/10.1016/j.ophtha.2006.04.022.
3. Chong, W.P., Horai, R., Mattapallil, M.J., Silver, P.B., Chen, J., Zhou, R., Sergeev, Y., Villasmil, R., Chan, C.C., and Caspi, R.R. (2014). IL-27p28 inhibits central nervous system autoimmunity by concurrently antagonizing Th1 and Th17 responses. J. Autoimmun. *50*, 12–22. https://doi.org/10.1016/j.jaut.2013.08.003.
4. Zeboulon, N., Dougados, M., and Gossec, L. (2008). Prevalence and characteristics of uveitis in the spondyloarthropathies: a systematic literature review. Ann. Rheum. Dis. *67*, 955–959. https://doi.org/10.1136/ard.2007.075754.
5. Tseng, S.T., Yao, T.C., Huang, J.L., Yeh, K.W., and Hwang, Y.S. (2017). Clinical manifestations in uveitis patients with and without rheumatic disease in a Chinese population in Taiwan. J. Microbiol. Immunol. Infect. *50*, 798–804. https://doi.org/10.1016/j.jmii.2015.10.007.
6. Pennesi, G., Mattapallil, M.J., Sun, S.H., Avichezer, D., Silver, P.B., Karabekian, Z., David, C.S., Hargrave, P.A., McDowell, J.H., Smith, W.C., et al. (2003). A humanized model of experimental autoimmune uveitis in HLA class II transgenic mice. J. Clin. Invest. *111*, 1171–1180. https://doi.org/10.1172/jci15155.
7. Weindruch, R., and Sohal, R.S. (1997). Seminars in medicine of the Beth Israel Deaconess Medical Center. N. Engl. J. Med. *337*, 986–994. https://doi.org/10.1056/nejm199710023371407.
8. Kökten, T., Hansmannel, F., Ndiaye, N.C., Heba, A.C., Quilliot, D., Dreumont, N., Arnone, D., and Peyrin-Biroulet, L. (2021). Calorie Restriction as a New Treatment of Inflammatory Diseases. Adv. Nutr. *12*, 1558–1570. https://doi.org/10.1093/advances/nmaa179.
9. Harlé, G., Kowalski, C., Garnier, L., and Hugues, S. (2020). Lymph Node Stromal Cells: Mapmakers of T Cell Immunity. Int. J. Mol. Sci. *21*, 7785. https://doi.org/10.3390/ijms21207785.
10. Saxena, V., Li, L., Paluskievicz, C., Kasinath, V., Bean, A., Abdi, R., Jewell, C.M., and Bromberg, J.S. (2019). Role of lymph node stroma and microenvironment in T cell tolerance. Immunol. Rev. *292*, 9–23. https://doi.org/10.1111/imr.12799.
11. Phillips, M.J., Needham, M., and Weller, R.O. (1997). Role of cervical lymph nodes in autoimmune encephalomyelitis in the Lewis rat. J. Pathol. *182*, 457–464. https://doi.org/10.1002/(sici)1096-9896(199708)182:4<457::Aid-path870>3.0.Co;2-y.
12. Gasteiger, G., Ataide, M., and Kastenmüller, W. (2016). Lymph node - an organ for T-cell activation and pathogen defense. Immunol. Rev. *271*, 200–220. https://doi.org/10.1111/imr.12399.
13. Louveau, A., Herz, J., Alme, M.N., Salvador, A.F., Dong, M.Q., Viar, K.E., Herod, S.G., Knopp, J., Setliff, J.C., Lupi, A.L., et al. (2018). CNS lymphatic drainage and neuroinflammation are regulated by meningeal lymphatic vasculature. Nat. Neurosci. *21*, 1380–1391. https://doi.org/10.1038/s41593-018-0227-9.
14. Zenz, R., Eferl, R., Scheinecker, C., Redlich, K., Smolen, J., Schonthaler, H.B., Kenner, L., Tschachler, E., and Wagner, E.F. (2008). Activator protein 1 (Fos/Jun) functions in inflammatory bone and skin disease. Arthritis Res. Ther. *10*, 201. https://doi.org/10.1186/ar2338.
15. Novoszel, P., Holcmann, M., Stulnig, G., De Sa Fernandes, C., Zyulina, V., Borek, I., Linder, M., Bogusch, A., Drobits, B., Bauer, T., et al. (2021). Psoriatic skin inflammation is promoted by c-Jun/AP-1-dependent CCL2 and IL-23 expression in dendritic cells. EMBO Mol. Med. *13*, e12409. https://doi.org/10.15252/emmm.202012409.
16. Karakaslar, E.O., Katiyar, N., Hasham, M., Youn, A., Sharma, S., Chung, C.H., Marches, R., Korstanje, R., Banchereau, J., and Ucar, D. (2023). Transcriptional activation of Jun and Fos members of the AP-1 complex is a conserved signature of immune aging that contributes to inflammaging. Aging Cell *22*, e13792. https://doi.org/10.1111/acel.13792.
17. Wu, S., Ma, R., Zhong, Y., Chen, Z., Zhou, H., Zhou, M., Chong, W., and Chen, J. (2021). Deficiency of IL-27 Signaling Exacerbates Experimental Autoimmune Uveitis with Elevated Uveitogenic Th1 and Th17 Responses. Int. J. Mol. Sci. *22*, 7517. https://doi.org/10.3390/ijms22147517.
18. DeYoung, M.P., Horak, P., Sofer, A., Sgroi, D., and Ellisen, L.W. (2008). Hypoxia regulates TSC1/2-mTOR signaling and tumor suppression through REDD1-mediated 14-3-3 shuttling. Genes Dev. *22*, 239–251. https://doi.org/10.1101/gad.1617608.
19. Khan, M.M., Kalim, U.U., Khan, M.H., and Lahesmaa, R. (2021). PP2A and Its Inhibitors in Helper T-Cell Differentiation and Autoimmunity. Front. Immunol. *12*, 786857. https://doi.org/10.3389/fimmu.2021.786857.
20. Stambolic, V., Suzuki, A., de la Pompa, J.L., Brothers, G.M., Mirtsos, C., Sasaki, T., Ruland, J., Penninger, J.M., Siderovski, D.P., and Mak, T.W. (1998). Negative regulation of PKB/Akt-dependent cell survival by the tumor suppressor PTEN. Cell *95*, 29–39. https://doi.org/10.1016/s0092-8674(00)81780-8.
21. Chen, J., and Caspi, R.R. (2019). Clinical and Functional Evaluation of Ocular Inflammatory Disease Using the Model of Experimental Autoimmune Uveitis. Methods Mol. Biol. *1899*, 211–227. https://doi.org/10.1007/978-1-4939-8938-6_15.
22. Luger, D., Silver, P.B., Tang, J., Cua, D., Chen, Z., Iwakura, Y., Bowman, E.P., Sgambellone, N.M., Chan, C.C., and Caspi, R.R. (2008). Either a Th17 or a Th1 effector response can drive autoimmunity: conditions of disease induction affect dominant effector category. J. Exp. Med. *205*, 799–810. https://doi.org/10.1084/jem.20071258.
23. Yasuda, K., Takeuchi, Y., and Hirota, K. (2019). The pathogenicity of Th17 cells in autoimmune diseases. Semin. Immunopathol. *41*, 283–297. https://doi.org/10.1007/s00281-019-00733-8.
24. Jiang, G., Sun, D., Yang, H., Lu, Q., Kaplan, H.J., and Shao, H. (2014). HMGB1 is an early and critical mediator in an animal model of uveitis induced by IRBP-specific T cells. J. Leukoc. Biol. *95*, 599–607. https://doi.org/10.1189/jlb.0613337.
25. Zahoor, I., Suhail, H., Datta, I., Ahmed, M.E., Poisson, L.M., Waters, J., Rashid, F., Bin, R., Singh, J., Cerghet, M., et al. (2022). Blood-based untargeted metabolomics in relapsing-remitting multiple sclerosis revealed the testable therapeutic target. Proc. Natl. Acad. Sci. USA *119*, e2123265119. https://doi.org/10.1073/pnas.2123265119.
26. Locasale, J.W. (2013). Serine, glycine and one-carbon units: cancer metabolism in full circle. Nat. Rev. Cancer *13*, 572–583. https://doi.org/10.1038/nrc3557.
27. Abe, T., Nakajima, A., Satoh, N., Ohkoshi, M., Sakuragi, S., and Koizumi, A. (2001). Suppression of experimental autoimmune uveoretinitis by dietary calorie restriction.

Jpn. J. Ophthalmol. *45*, 46–52. https://doi.org/10.1016/s0021-5155(00)00303-8.
28. Guarente, L. (2013). Calorie restriction and sirtuins revisited. Genes Dev. *27*, 2072–2085. https://doi.org/10.1101/gad.227439.113.
29. Mercken, E.M., Crosby, S.D., Lamming, D.W., JeBailey, L., Krzysik-Walker, S., Villareal, D.T., Capri, M., Franceschi, C., Zhang, Y., Becker, K., et al. (2013). Calorie restriction in humans inhibits the PI3K/AKT pathway and induces a younger transcription profile. Aging Cell *12*, 645–651. https://doi.org/10.1111/acel.12088.
30. Cantó, C., and Auwerx, J. (2011). Calorie restriction: is AMPK a key sensor and effector? Physiology *26*, 214–224. https://doi.org/10.1152/physiol.00010.2011.
31. Yong-Quan Ng, G., Yang-Wei Fann, D., Jo, D.G., Sobey, C.G., and Arumugam, T.V. (2019). Dietary Restriction and Epigenetics: Part I. Cond. Med. *2*, 284–299.
32. Eltzschig, H.K., and Carmeliet, P. (2011). Hypoxia and inflammation. N. Engl. J. Med. *364*, 656–665. https://doi.org/10.1056/NEJMra0910283.
33. D'Ignazio, L., Bandarra, D., and Rocha, S. (2016). NF-κB and HIF crosstalk in immune responses. FEBS J. *283*, 413–424. https://doi.org/10.1111/febs.13578.
34. Malinowski, B., Zalewska, K., Węsierska, A., Sokołowska, M.M., Socha, M., Liczner, G., Pawlak-Osińska, K., and Wiciński, M. (2019). Intermittent Fasting in Cardiovascular Disorders-An Overview. Nutrients *11*, 673. https://doi.org/10.3390/nu11030673.
35. Ma, S., Sun, S., Geng, L., Song, M., Wang, W., Ye, Y., Ji, Q., Zou, Z., Wang, S., He, X., et al. (2020). Caloric Restriction Reprograms the Single-Cell Transcriptional Landscape of Rattus Norvegicus Aging. Cell *180*, 984–1001.e22. https://doi.org/10.1016/j.cell.2020.02.008.
36. Anekonda, T.S. (2009). The Benefits of Calorie Restriction and Calorie Restriction Mimetics as Related to the Eye. Open Longev. Sci. *3*, 28–37. https://doi.org/10.2174/1876326x00903020028.
37. Kawashima, M., Ozawa, Y., Shinmura, K., Inaba, T., Nakamura, S., Kawakita, T., Watanabe, M., and Tsubota, K. (2013). Calorie restriction (CR) and CR mimetics for the prevention and treatment of age-related eye disorders. Exp. Gerontol. *48*, 1096–1100. https://doi.org/10.1016/j.exger.2013.04.002.
38. Guo, X., Kimura, A., Azuchi, Y., Akiyama, G., Noro, T., Harada, C., Namekata, K., and Harada, T. (2016). Caloric restriction promotes cell survival in a mouse model of normal tension glaucoma. Sci. Rep. *6*, 33950. https://doi.org/10.1038/srep33950.
39. Feng, J., Zhang, S., Li, W., Bai, T., Liu, Y., and Chang, X. (2022). Intermittent Fasting to the Eye: A New Dimension Involved in Physiological and Pathological Changes. Front. Med. *9*, 867624. https://doi.org/10.3389/fmed.2022.867624.
40. Zhong, Z., Su, G., Kijlstra, A., and Yang, P. (2021). Activation of the interleukin-23/interleukin-17 signalling pathway in autoinflammatory and autoimmune uveitis. Prog. Retin. Eye Res. *80*, 100866. https://doi.org/10.1016/j.preteyeres.2020.100866.
41. Huang, Z., Li, W., and Su, W. (2021). Tregs in Autoimmune Uveitis. Adv. Exp. Med. Biol. *1278*, 205–227. https://doi.org/10.1007/978-981-15-6407-9_11.
42. Butler, A., Hoffman, P., Smibert, P., Papalexi, E., and Satija, R. (2018). Integrating single-cell transcriptomic data across different conditions, technologies, and species. Nat. Biotechnol. *36*, 411–420. https://doi.org/10.1038/nbt.4096.
43. Zhou, Y., Zhou, B., Pache, L., Chang, M., Khodabakhshi, A.H., Tanaseichuk, O., Benner, C., and Chanda, S.K. (2019). Metascape provides a biologist-oriented resource for the analysis of systems-level datasets. Nat. Commun. *10*, 1523. https://doi.org/10.1038/s41467-019-09234-6.
44. Chan, C.C., Caspi, R.R., Ni, M., Leake, W.C., Wiggert, B., Chader, G.J., and Nussenblatt, R.B. (1990). Pathology of experimental autoimmune uveoretinitis in mice. J. Autoimmun. *3*, 247–255. https://doi.org/10.1016/0896-8411(90)90144-h.
45. Agarwal, R.K., Silver, P.B., and Caspi, R.R. (2012). Rodent models of experimental autoimmune uveitis. Methods Mol. Biol. *900*, 443–469. https://doi.org/10.1007/978-1-60761-720-4_22.
46. Li, H., Xie, L., Zhu, L., Li, Z., Wang, R., Liu, X., Huang, Z., Chen, B., Gao, Y., Wei, L., et al. (2022). Multicellular immune dynamics implicate PIM1 as a potential therapeutic target for uveitis. Nat. Commun. *13*, 5866. https://doi.org/10.1038/s41467-022-33502-7.
47. Mor, F., Quintana, F., Mimran, A., and Cohen, I.R. (2003). Autoimmune encephalomyelitis and uveitis induced by T cell immunity to self beta-synuclein. J. Immunol. *170*, 628–634. https://doi.org/10.4049/jimmunol.170.1.628.
48. Wu, Y., Yang, S., Ma, J., Chen, Z., Song, G., Rao, D., Cheng, Y., Huang, S., Liu, Y., Jiang, S., et al. (2022). Spatiotemporal Immune Landscape of Colorectal Cancer Liver Metastasis at Single-Cell Level. Cancer Discov. *12*, 134–153. https://doi.org/10.1158/2159-8290.Cd-21-0316.
49. Vento-Tormo, R., Efremova, M., Botting, R.A., Turco, M.Y., Vento-Tormo, M., Meyer, K.B., Park, J.E., Stephenson, E., Polański, K., Goncalves, A., et al. (2018). Single-cell reconstruction of the early maternal-fetal interface in humans. Nature *563*, 347–353. https://doi.org/10.1038/s41586-018-0698-6.
50. Huynh-Thu, V.A., Irrthum, A., Wehenkel, L., and Geurts, P. (2010). Inferring regulatory networks from expression data using tree-based methods. PLoS One *5*, e12776. https://doi.org/10.1371/journal.pone.0012776.
51. Verfaillie, A., Imrichova, H., Janky, R., and Aerts, S. (2015). iRegulon and i-cisTarget: Reconstructing Regulatory Networks Using Motif and Track Enrichment. Curr. Protoc. Bioinf. *52*, 2.16.1–2.16.39. https://doi.org/10.1002/0471250953.bi0216s52.
52. Aibar, S., González-Blas, C.B., Moerman, T., Huynh-Thu, V.A., Imrichova, H., Hulselmans, G., Rambow, F., Marine, J.C., Geurts, P., Aerts, J., et al. (2017). SCENIC: single-cell regulatory network inference and clustering. Nat. Methods *14*, 1083–1086. https://doi.org/10.1038/nmeth.4463.

STAR★METHODS

KEY RESOURCES TABLE

REAGENT or RESOURCE	SOURCE	IDENTIFIER
Antibodies		
Zombie NIR	Biolegend	Cat#: 423106
CD4	Biolegend	Cat#: 100434
IL17A	Biolegend	Cat#: 506912
GM-CSF	Biolegend	Cat#: 505411
CD25	Biolegend	Cat#: 102016
IFN-γ	Biolegend	Cat#: 505808
Foxp3	eBioscience	Cat#: 11-5773-82
RORγt	BD Pharmingen	Cat#: 562682
p-Pi3k	ThermoFisher	Cat#: MA528027
p-Akt	Biolegend	Cat#: 606554
c-Myc	Novus	Cat#: NB600-302PE
HK2	Abcam	Cat#: ab237314
LDHA	Abcam	Cat#: ab210445
PKM2	Abcam	Cat#: ab210448
Chemicals, peptides, and recombinant proteins		
RPMI 1640 culture medium	GIBCO	Cat#: 11875119
DMEM/F-12 (1:1) basic (1X)	GIBCO	LOT# 8119025
Fetal Bovine Serum (FBS), qualified, Australia	GIBCO	Cat# 10099141C
Collagenase II	GIBCO	Cat#17101-015
DNase I	Sigma-Aldrich	Cat#DN25
Phosphate Buffer Saline (PBS, 1X)	CORNING	LOT# 21020007
Tissue-Tek O.C.T Compound	Sakura Finetek USA, Inc	LOT# 0565-00
Penicillin-streptomycin	GIBCO	Cat#: 15070063
IRBP1-20	GiL Biochem	Cat#: 051038
complete Freund's adjuvant	BD Difco	Cat#: SLCC1714
Mycobacterium tuberculosis strain H37Ra	BD Difco	Cat#: 1294163
PTX	Sigma-Aldrich	Cat#: 180242A1
Phorbol 12-myristate 13-acetate (PMA)	Sigma	Cat#: P8139
Ionomycin calcium salt	Sigma	Cat#: I3909
Brefeldin A (BFA)	Selleck	Cat#: S7046
Critical commercial assays		
Chromium Single Cell 3′ Library & Gel Bead Kit v2	10X Genomics	Cat#PN-120237
Deposited data		
Raw data files files for scRNA-seq	This study	GSA: CRA016398
Software and algorithms		
Cell Ranger (version: 5.0.0)	10x Genomics	https://support.10xgenomics.com/single-cell-gene-expression/software/downloads/latest
Loupe Browser (version: 5.0.0)	10x Genomics	https://support.10xgenomics.com/single-cellgene-expression/software/downloads/latest

(*Continued on next page*)

Continued

REAGENT or RESOURCE	SOURCE	IDENTIFIER
R (version: 4.3.0)	R Core	https://www.r-project.org/
Seurat (version: 4.0.1)	Butler et al., 2018[42]	https://satijalab.org/seurat/
Harmony (version 2.0.4)	Korsunsky et al., 2019	https://github.com/pardeike/Harmony
Metascape (version: 3.5)	Zhou et al., 2019[43]	http://metascape.org/
Monocle (version: 2.99.3)	Qiu et al., 2017	http://cole-trapnell-lab.github.io/monocle-release/docs/
CellPhoneDB 2	Github	https://github.com/ventolab/CellphoneDB
pheatmap (version: 1.0.12)	N/A	https://cran.r-project.org/web/packages/pheatmap/index.html
ggplot2 (version: 3.2.1)	Wickham, 2016	https://ggplot2.tidyverse.org/
ImageJ (version: 1.8.0)	NIH	https://imagej.nih.gov/ij/
GraphPad Prism 8	GraphPad Software Inc.	https://www.graphpad.com/scientific-software/prism/

EXPERIMENTAL MODEL AND STUDY PARTICIPANT DETAILS

Mice

C57BL/6J mice (6 weeks old) were obtained from the Medical Lab Animal Center (Guangzhou, China). Both normal and EAU mice were housed in a specific pathogen-free environment at 21 ± 1°C and 60 ± 5% humidity, with a 12-hour light/dark cycle. All animal experiments followed the Association for Research in Vision and Ophthalmology (ARVO) statement and institutional policies for animal use of Zhongshan Ophthalmic Center, Sun Yat-Sen University (ethical approval number: O2022060).

METHOD DETAILS

Caloric restriction

Female mice, aged 6 weeks, were fed AL for 14 days before initiating the regimens of CR. Subsequently, the mice were randomly assigned to distinct CR groups and kept individually in cages. The AL mice continued to be fed regular chow, while CR mice received 40% less compared to the baseline intake of AL mice. After 28 days of CR, both AL and CR mice were randomly assigned to receive or not receive induction of the EAU model (n = 6 mice/group). At day 42 of CR, with or without EAU, the mice were sacrificed. CDLNs together with spleens were aseptically removed, followed by the analysis for scRNA-seq and flow cytometry.

EAU model induction and clinical score

EAU was induced in mice by subcutaneous injection of an emulsion containing 2 mg/mL of retinal antigen interphotoreceptor retinoid-binding protein 1-20 ($IRBP_{1-20}$) (GiL Biochem, Shanghai, China) and complete Freund's adjuvant (BD Difco, San Jose, CA, USA), with 2.5 mg of Mycobacterium tuberculosis strain H37Ra (BD Difco, San Jose, CA, USA) in a 1:1 volume ratio. In addition, 0.25 μg of pertussis toxin (PTX) (List Biological Laboratories, Campbell, California, USA) dissolved in PBS was injected on the same day and 2 days after immunization.[21,44,45]

The progression of EAU was observed using the Micron IV fundus camera (Phoenix Co., Campbell, CA, USA), and clinical findings were graded from 0 to 4 according to observable infiltration and vasculitis in the retina.[45,46]

Histopathologic assessment

On day 14 after immunization, mice were euthanized, with their eyeballs harvested and immersed in 4% paraformaldehyde for a duration of 48 hours. Subsequently, eyeballs were embedded in paraffin, stained with hematoxylin and eosin (H&E), and assessed for pathological scores using a blinded method.[21]

Treatment of CDLNs

On day 14 following immunization, CDLN cells were isolated from the EAU-AL (EAU-AL) group as well as EAU-CR (EAU-CR) group. These cells were treated with $IRBP_{1-20}$ (20 μg/mL) at the temperature of 37°C for a duration of 72 hours, followed by flow cytometry analysis of cell samples. Alternative method to induce $IRBP_{1-20}$-specific T cells is described in the previous study.[24]

Flow cytometry analysis

Cells from the retina and CDLNs were collected, washed with live or dead dye (#423105) and phosphate buffered saline (PBS), and stained with the following antibodies: CD4 (PerCP/Cy5.5, #100434), CD25 (PE/Cy7, #102016). For intracellular cytokine staining, cells were stimulated with phorbol myristate acetate (5 ng/mL), ionomycin (500 ng/mL), and brefeldin A (1 μg/mL) (Sigma) at 37°C for a duration of 5 h. Following

fixation as well as permeabilization, cells were then stained with antibodies: IFN-γ (PE, #505808), IL-17A (AF647, #506912), Foxp3 (FITC, #11-5773-82), and Granulocyte-macrophage Colony Stimulating Factor (GM-CSF) (PE/Cy7, #505411). The measurement and analysis of cells were carried out utilizing FlowJo software (version 10.0.7, USA).

Adoptive transfer of $CD4^+$ TCs

CDLN cells obtained from the EAU-AL or EAU-CR group were cultured with 20 μg/mL of $IRBP_{1-20}$ for a duration of 72 hours. Subsequently, the sorted $CD4^+$ TCs were injected into naïve mice (2×10^7 cells for each mouse).[47]

scRNA sequencing and analysis

Single-cell suspensions from CDLN samples were utilized to generate barcoded scRNA-seq libraries through the Chromium Single Cell 3′ Reagent v2 kits (10X Genomics). The raw data was processed using the "cellranger count" function from CellRanger version 5.0.0 (10X Genomics) to demultiplex cellular barcodes, map reads to the mouse reference genome (mm10, 10X Genomics), and generate a raw unique molecular identifier count matrix. The normalized aggregate data across samples was generated using the "cellranger aggr" function. Using the R package Seurat[42] (version 4.0.1), the resulting count matrix was then converted into a Seurat object. To ensure data quality, mitochondrial transcripts were restricted to less than 15%. Besides, the identified gene number in each cell was limited to fewer than 200 to eliminate potential cell debris or doublets. Known biological cell types were assigned to each cell utilizing conventional markers described previously. The "FindAllMarker()" function was employed to identify preferentially expressed genes within clusters or DEGs between the cells from different groups.

DEG analysis

The 'FindMarkers' function was utilized to conduct DEG analysis for different cell types between different groups (NR/NA, EAU-CR/EAU-AL). DEGs were defined as having an adjusted P value less than 0.05 and |LogFC| over 0.25. Prior to the DEG analysis, cell types with missing values or fewer than three cells were excluded from the groups.

Gene Ontology (GO) enrichment analysis

DEGs underwent GO and pathway enrichment analysis utilizing the Metascape webtool (www.metascape.org).[43] The FDR was calculated using the Benjamini-Hochberg procedure to account for multiple testing. The pheatmap (v1.0.12) as well as ggplot2 package (v3.2.1) were used to visualize 5-10 GO terms or pathways related with CR or EAU among the top 100 enriched GO terms across distinct cell types.

Metabolic pathway analysis

Single-cell metabolic activity was quantified as metabolic pathway score using scMetabolism R package.[48] Among the 85 metabolic Kyoto Encyclopedia of Genes and Genomes pathways along with 82 REACTOME metabolic pathways, this study focused on glycolysis/gluconeogenesis, citrate (TCA) cycle, and oxidative phosphorylation pathways.

Cell–cell communication analysis with CellPhoneDB 2

As a Python-based computational analysis tool developed by Roser Vento-Tormo et al.,[49] CellPhoneDB 2 was employed to analyze molecular interactions in cell-cell communication. Ligand-receptor pairs present in over 10% of a given cell type were selected and analyzed. The mean expression of ligand-receptor pairs among distinct cell types was compared, and pairs with P less than 0.05 were subsequently examined for intercellular communication.

Transcriptional factor (TF)

To identify TFs, the workflow (http://scenic.aertslab.org/) was followed. TF-binding motifs were determined using the GENIE3 packages (version 1.6.0)[50] and the RcisTarget database (version 1.4.0)[51] of the SCENIC (version 1.1.2.2).[52] TFs were considered active if they were found in over 1% of all cells and linked to at least one other regulon (|r| more than 0.3).

QUANTIFICATION AND STATISTICAL ANALYSIS

Statistics

The statistical analysis in our study involved using various tests depending on the specific comparison. Student's t-test (unpaired, two-tailed) was employed for some analyses, while a one-way ANOVA or Wilcoxon rank-sum test was used for others. To compare expression values, we utilized the Seurat function "FindMarkers()". Cell type markers were determined using the "FindAllMarkers()" function with a negative binomial test. Statistical analyses and graphical representations were conducted utilizing R (version 4.3.0) as well as GraphPad Prism (version 8.0.2). Adjusted p-values higher than 0.05 indicated not significant (ns), while significance levels were represented as follows: *, $P < 0.05$; **, $P < 0.01$; ***, $P < 0.001$; and ****, $P < 0.0001$.